PINN Approximation of Steady 2D Flow Past a Square Cylinder

Yash Ramchandra Bagwe Manasi[1], Bibek Dhungana[2], Chandan Bose[3], Parees Palkar[4] and Evan Fernandes[5]

[1]Department of Mechanical Engineering, K.J. Somaiya School of Engineering

[2]Department of Mechanical Engineering, Tribhuvan University

[3] Department of Aerospace Engineering, The University of Birmingham

[4]Project Research Assistant, IIT Bombay

[5]Project Research Assistant, IIT Bombay

Abstract

In recent years, physics-informed neural networks have become a popular mesh-free method of solving physics equations in fluid mechanics, and they are associated with some benefits compared to traditional discretization methods. This study examines how PINNs, through the DeepXDE model, can be used to model steady two-dimensional incompressible laminar flow around a square cylinder at Reynolds number 10, 20, and 30. The neural network loss is implemented with the Navier-Stokes and continuity equations as constraints, geometric constraints and boundary conditions to ensure physical consistency. This study creates an authenticated framework system with mesh-free CFD application in laminar regime.

Table of Contents

List of Figures

List of Tables

List of Equations

1. Introduction

1.1 Background of the Topic

The conventional mesh-based solvers are used to predict bluff body flows, and, in this case, computational overhead is substantial due to the need to perform repeated runs to optimize, quantify uncertainty, or study parameters. Computational fluid dynamics (CFD) is the conventional tool used to predict bluff body flows, but with repeated simulations being necessary, more computationally expensive solvers are required. The geometrically simple square cylinder has separated-flow physics boundary-layers, flow separation, formation of recirculation zones, and recovery of pressure, and is a classical CFD test case. In low Reynolds number (Re <50) the flow is steady and two dimensional with architecture physics well-understood and presents the ideal validation environment against new computational methods.

The recent developments of neural network-based surrogate modelling have the potential to lower the computational cost and estimate high-fidelity flow fields. Physics-Informed Neural Networks PINNs are a potential type of surrogate models which encompasses partial differential equations into the learning mechanism via automatic differentiation. In contrast to purely data-driven methods that need huge dataset, PINNs can incorporate Navier-Stokes equations and continuity constraints as soft physics constraints in the loss function, allowing the approximation of the flow field to be done with the help of moderate quantities of CFD generated training data. More importantly, PINNs can be mesh-free, which is that only collocation points are discretized, and it is not a mesh that is imposed on the space, which may introduce a computational efficiency advantage when training.

One of the most important research questions is as follows: Can PINNs be used to predict the contours and spatial distributions of the velocity and pressure fields of the bluff body flows? PINN studies have been previously shown to be valid against CFD on canonical benchmarks, though the analysis of contour-level accuracy and detailed visualization of square cylinder flows at a variety of Reynolds numbers remains very scarce.

1.2 Motivation of the Study

The computational cost associated with traditional CFD methods can become prohibitive when multiple simulations are required for optimization or sensitivity analyses. Purely data-driven deep learning approaches typically demand large volumes of training data and do not inherently enforce physical conservation laws. Physics-Informed Neural Networks (PINNs) address these limitations by embedding the governing equations directly into the loss function, resulting in

significantly improved data efficiency compared to supervised learning. Key advantages of PINNs include reduced training data requirements, adherence to physical conservation principles, a mesh-free formulation that eliminates the need for expensive grid generation, and rapid inference times on the order of milliseconds, as opposed to hours for conventional CFD simulations

Objective: Bridge the gap between ML and CFD while determining whether PINNs can reliably model and visualize the flow field contours around a square cylinder for 2D laminar bluff-body problems.

1.3 Literature Review

Physics-Informed Neural Networks (Raissi et al. 2019) represent a significant advancement in the field of scientific modelling because they leave the realm of data-driven neural networks and enter the world of physics-informed neural networks. The integration of the partial differential equations (PDEs) into training of the neural networks using automatic differentiation is noteworthy in this shift. Trade-offs between PDE residual and supervised learning via weighted loss functions and multi-fidelity schemes in hybrid physics-data methods have resulted in the fact that convergence and quality of solutions in hybrid physics-informed and data-driven schemes have dramatically improved. The studies of invalidation have demonstrated that fields of predicted velocity and pressure are consistent with high-order CFD solvers within 1-2 per cent margin error, and they are able to capture the structures of the flow, such as the boundary layer and wake. A more recent trend in the literature is devoted to problem-specific comprehensive analysis to identify the situations when PINNs provide actual computational advantages over classical CFD and the other way around. Even though PINNs are yet to be seen as a possible complementary solver, systematic studies regarding steady laminar bluff-body flows at various Reynolds number using hybrid training and detailed CFD comparison are still lacking, hence the extensive baselines of validation is to be established.

2. Problem Statement

The problem of flow around a square cylinder is represented by a rectangular channel with a square obstacle of dimensions 1m × 1m positioned at coordinates (10.5, 10.5). The dimensions of the domain are given as x = 31L and y = 21L where L = 1m is the side length.

Flow Classification:

The flow is considered incompressible and laminar. The Reynolds number is defined by the formula Re=UL/ν, where U = 1 m/s (inlet velocity), L = 1m (characteristic length), and ν (kinematic viscosity). Three values of the Reynolds number are studied:

Re = 10 (ν = 0.1)

Re = 20 (ν = 0.05)

Re = 30 (ν = 0.033)

3. Governing Equations

In this study, fluid movement is controlled by the steady incompressible Navier-Stokes equations, which are the representation of the conservation of mass and momentum for a Newtonian fluid. The governing equations for an incompressible fluid of constant density are expressed in vector form as:

$$\nabla \cdot \mathbf{u} = 0 \tag{1}$$

$$(\mathbf{u} \cdot \nabla)\mathbf{u} = -\frac{1}{\rho}\nabla p + \nu\nabla^2\mathbf{u} \tag{2}$$

where $\mathbf{u} = (u, v)$is the velocity vector, $p$is the kinematic pressure, $\rho$is the fluid density, and $\nu$is the kinematic viscosity. Mass conservation is enforced by Equation (1), which necessitates that the velocity field possesses zero divergence throughout the entire domain. Momentum representation is the inertial force, pressure force, and viscous force balance as expressed in Equation (2) which is the momentum equation.

Expanding equations (1) and (2) in Cartesian coordinates produces the following PDE system:

Continuity Equation:

$$\frac{\partial u}{\partial x} + \frac{\partial v}{\partial y} = 0 \tag{3}$$

x-Momentum Equation:

$$\rho\left(u\frac{\partial u}{\partial x}+v\frac{\partial u}{\partial y}\right)=-\frac{\partial p}{\partial x}+\nu\left(\frac{\partial^2 u}{\partial x^2}+\frac{\partial^2 u}{\partial y^2}\right) \quad (4)$$

y-Momentum Equation:

$$\rho\left(u\frac{\partial v}{\partial x}+v\frac{\partial v}{\partial y}\right)=-\frac{\partial p}{\partial y}+\nu\left(\frac{\partial^2 u}{\partial x^2}+\frac{\partial^2 u}{\partial y^2}\right) \quad (5)$$

The mentioned equations are valid for the case of steady, laminar, incompressible flow appropriate for Reynolds numbers Re=10, 20 & 30.

Here ρ (fluid density) is considered constant since it's incompressible flow.

Within the Physics-Informed Neural Network framework, the DeepXDE's automatic differentiation computes all spatial derivatives required for the PDE residuals. The residuals corresponding to equations (3) to (5) become:

$$f_c=\frac{\partial u}{\partial x}+\frac{\partial v}{\partial y} \quad (6)$$

$$f_u=u\frac{\partial u}{\partial x}+v\frac{\partial u}{\partial y}+\frac{\partial p}{\partial x}-\nu\left(\frac{\partial^2 u}{\partial x^2}+\frac{\partial^2 u}{\partial y^2}\right) \quad (7)$$

$$f_v=u\frac{\partial v}{\partial x}+v\frac{\partial v}{\partial y}+\frac{\partial p}{\partial y}-\nu\left(\frac{\partial^2 v}{\partial x^2}+\frac{\partial^2 v}{\partial y^2}\right) \quad (8)$$

The PINN reduces the total of the squared residuals corresponding to the collocation points within the domain, in addition to the violations of the boundary conditions at certain places, to the extent that it becomes zero.

4. Computational Domain

4.1 Geometry

- Overall domain: $[0,31] \times [0,21]$ in non-dimensional units
- Square obstacle: $[10,11] \times [10,11]$
- Three-dimensional extrusion: ±0.0025 in z

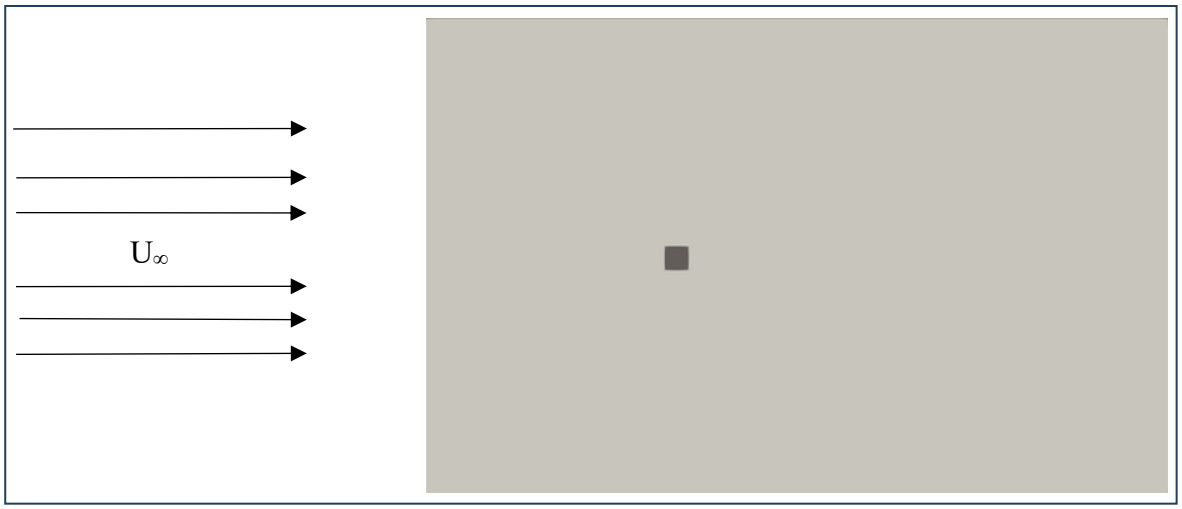

Figure 1: Computational geometry for the two-dimensional flow past a square cylinder with the flow entering from the left and exiting at the right boundary.

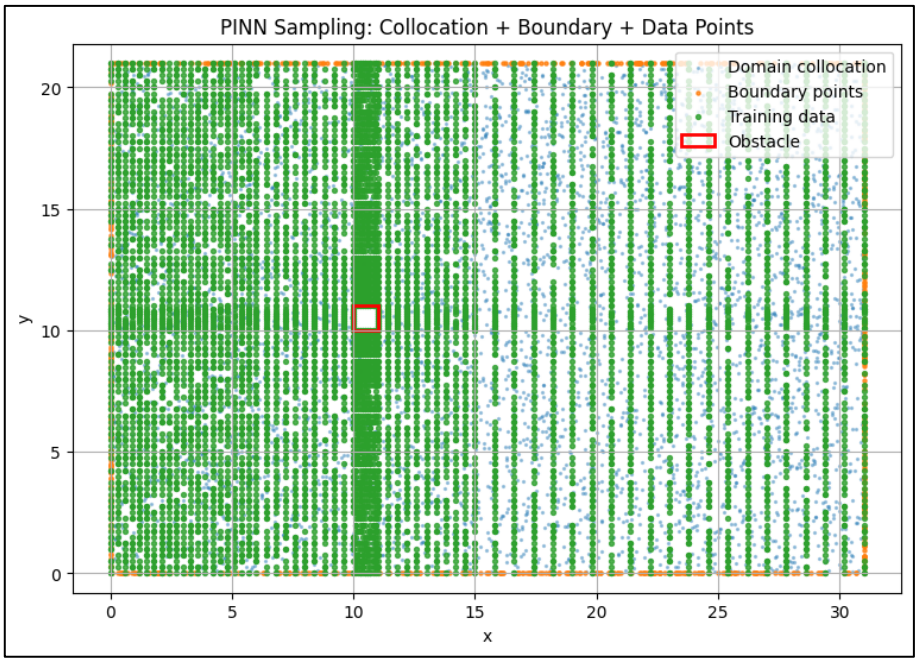

Figure 2: Distribution of points used in the Physics-Informed Neural Network (PINN) training process. The figure shows domain collocation points, boundary points, and supervised training data extracted from OpenFOAM simulation.

4.2 Mesh

OpenFOAM Mesh (based on blockMesh):

- Type of mesh: Structured hexagonal blocks with areas of refinement.
- Total cells: roughly 41,000 cells

Sampling for PINN:

- Mesh is not a required for PINN rather, the points of the training data are being sampled from OpenFOAM solution fields at discrete points.
- Training set includes 8,932 points while 1,914 points for validation set and testing

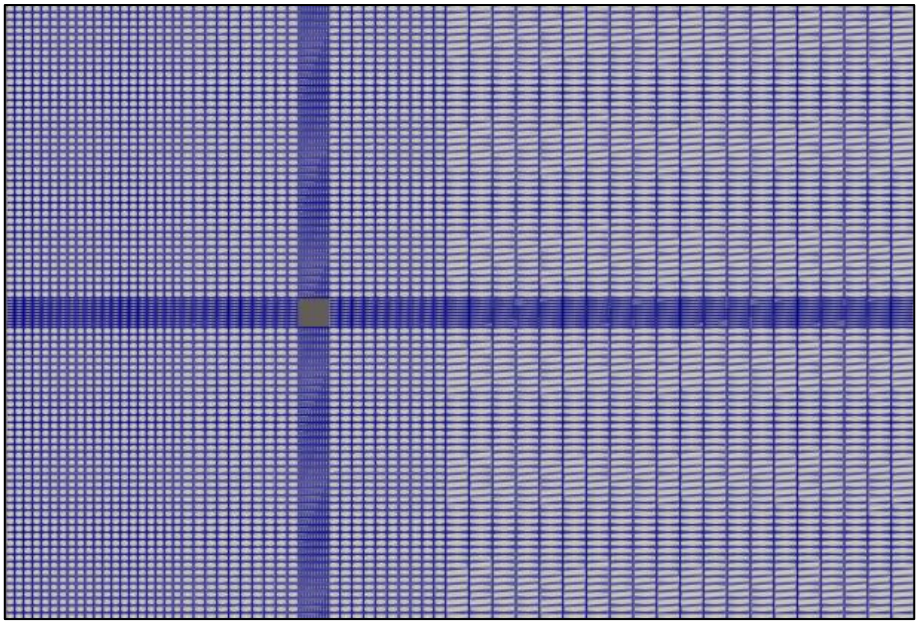

Figure 3: Structured computational mesh employed for the square cylinder flow simulations on OpenFOAM using blockMesh

4.3 Initial and Boundary Conditions

Velocity Conditions:

Table 1: Velocity boundary conditions.

Boundary	Condition	Value
Inlet (x = 0)	fixedValue	$\mathbf{u} = (1,0)$
Outlet (x = 31)	zeroGradient	-
Top/Bottom (y = 0, 21)	freestreamVelocity	$\mathbf{u} = (1,0)$
Obstacle Surface (square)	noSlip	$\mathbf{u} = (0,0)$

Pressure Boundary Conditions:

Table 2: Pressure boundary conditions.

Boundary	Condition
Inlet	zeroGradient
Outlet	fixedValue = 0
Walls (top/bottom/obstacle)	zeroGradient

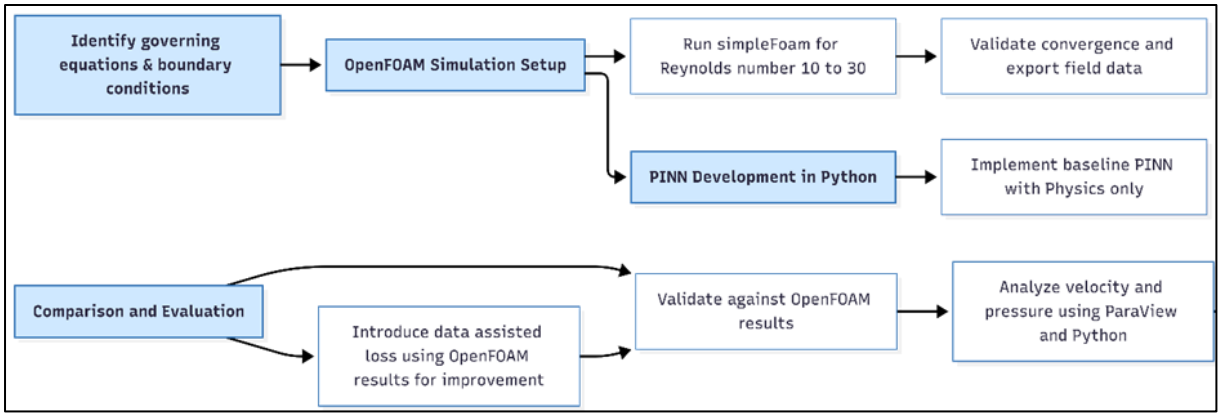

Figure 4: Workflow adopted in the present study for hybrid Physics-Informed Neural Network (PINN) development and validation. It includes OpenFOAM-based CFD simulations, PINN formulation and training, data-assisted loss integration, and systematic validation against reference CFD results.

4.4 Solver Selection

OpenFOAM**:**

Solver used was simpleFoam since it's steady-state incompressible flow with no transient terms. SIMPLE is robust and efficient for laminar, incompressible flows at low to moderate Reynolds numbers.

PINN**:**

- Framework: DeepXDE
- Backend: PyTorch
- Network type: Feedforward fully-connected neural network (FCNN)
- Advantage: No mesh required; continuous, differentiable approximation of flow fields

4.5 Discretization Schemes

The reference CFD solution is based on a finite-volume discretization of the OpenFOAM where gradients and diffusive terms are discretized using a second-order Gaussian scheme to provide central differences consistent with the Laplacian operator, though convective terms are discretized using div(phi,U) Gauss linearUpwind grad(U) to add an upwind bias to the numerical scheme to ensure stable numerical performance and in smooth regions, but does not use the opportunity to discretize the time derivative, so pseudo-time stepping is only used to effect a steady state of the SIMPLE iterations.

In contrast, the PINN does not rely on a spatial mesh or explicit discretization schemes.

4.6 Simulation Parameters

4.6.1 OpenFOAM Implementation:

Table 3: Control dictionary settings and convergence criteria used for steady-state OpenFOAM simulations.

Parameter	Value	Meaning
startTime	0	Begin pseudo-time at $t = 0$
endTime	5000	Run up to $t = 5000$ pseudo-time units
deltaT	1.0	Pseudo-time step
writeInterval	50	Write fields every 50 iterations
Residual tolerance (p)	10^{-4}	Pressure convergence criterion
Residual tolerance (U)	10^{-5}	Velocity convergence criterion

4.6.2 PINN Implementation:

PINN model is implemented as a fully–connected feed-forward neural network which takes spatial coordinates as input for prediction:

Network architecture:

Table 4: Architecture and hyperparameters of the Physics-Informed Neural Network (PINN).

Hyperparameter	Value
Input dimension	2 (x, y)
Hidden layers	6
Neurons per layer	60
Activation function	tanh
Output dimension	3 (u, v, p)
Weight initialization	Glorot normal

Optimization:

Table 5: Two-stage training strategy and optimizer settings used for PINN model training.

Phase	Optimizer	Learning rate	Iterations
Phase 1	Adam	1×10^{-4}	15,000
Phase 2	L-BFGS	line search	5,000 (until convergence)

The total loss in this work is a hybrid combination of physics, boundary, and data terms. The physics loss is defined from the steady incompressible Navier–Stokes residuals f_u, f_v, f_c, with a higher weight on continuity $(w_{f_u}, w_{f_v}, w_{f_c}) = (1,1,10)$ to strongly enforce incompressibility. Boundary conditions at the inlet, outlet, obstacle surface, and top/bottom walls are imposed via a separate loss with uniform weight $w_{\text{BC}} = 5$, ensuring the solution satisfies no-slip. A third, data-driven term compares the PINN prediction $(\text{u}, \text{v}, \text{p})$ against OpenFOAM data (Ux, Uy, p) at 8,932 training points using equal weights, i.e. $(w_u, w_v, w_p) = (1.5,1.5,1.5)$, which turns the model into a hybrid PINN by anchoring the solution to CFD data, especially in high-gradient regions around the obstacle.

Total loss and training time

The total hybrid loss is

$$\mathcal{L}_{\text{total}} = \mathcal{L}_{\text{PDE}} + \mathcal{L}_{\text{BC}} + \mathcal{L}_{\text{data}} \quad (9)$$

with the relative influence controlled by the weights as given above. Training for each Reynolds number took approximately 4520 seconds ($\approx$ 1.3 hours) on Google Colab using T4 GPU hardware accelerator.

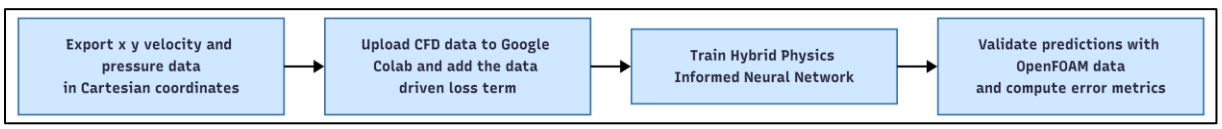

Figure 5: Workflow of the hybrid Physics-Informed Neural Network (PINN) formulation adopted.

DeepXDE Framework

DeepXDE framework and workflow: The hybrid PINN is developed in DeepXDE, which decomposes the definition of PDEs, geometry, boundary conditions and neural network training into individual modules.

The workflow is defined with the incompressible Navier–Stokes residuals using automatic differentiation; specify the rectangular domain around the square cylinder and the collocation/data points; impose Dirichlet conditions at inlet, outlet, obstacle, and top/bottom boundaries; construct a hybrid dataset combining residual, boundary, and OpenFOAM data points; define a fully connected network with six hidden layers and 60 neurons per layer with tanh activation; train the model using Adam followed by L-BFGS to minimise the loss

5. Results and Discussions

At Re = 10, the PINN converges smoothly, with train and test losses closely matched and a final test loss of $\mathcal{O}(10^{-2})$, indicating good generalization. For u_x, MAE = 0.0026, and R^2 = 0.9985; for v_y, MAE = 0.0012 and R^2 = 0.9967; for p, MAE = 0.0014 and R^2 = 0.9989. The divergence L_2 norm of 1.9×10^{-2} shows that incompressibility is enforced well.

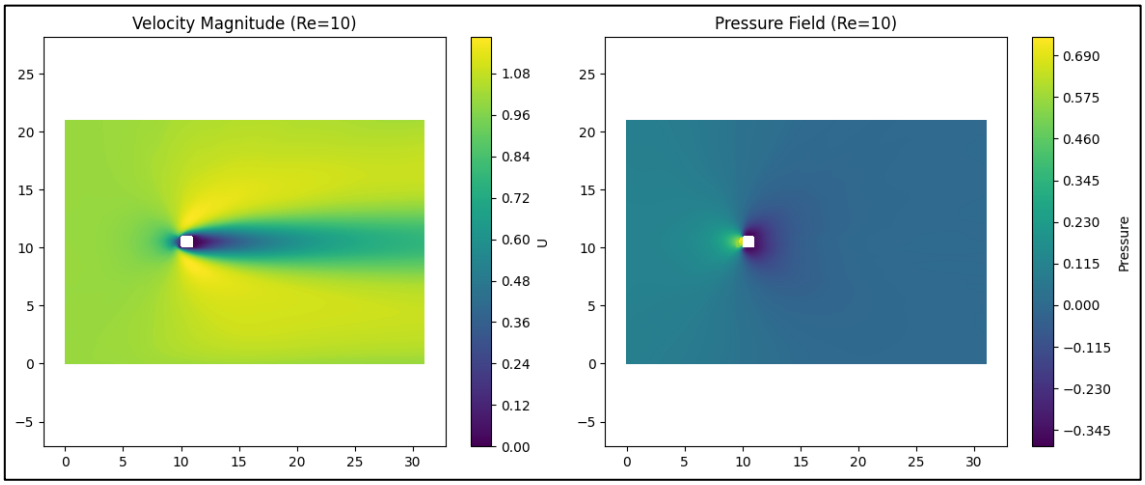

Figure 6: Velocity magnitude and pressure contours predicted by the Physics-Informed Neural Network (PINN) for Re = 10.

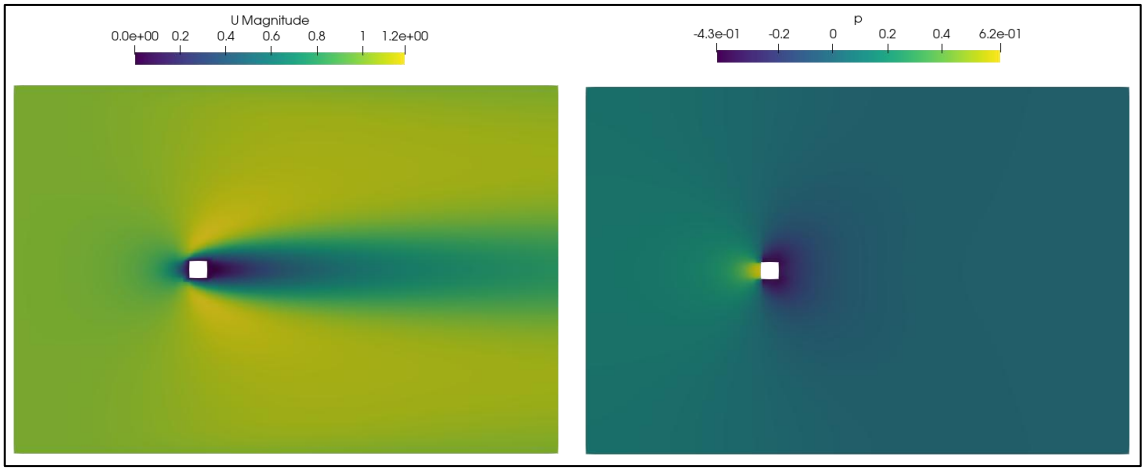

Figure 7: Velocity magnitude and pressure contours obtained from OpenFOAM simulations for Re10.

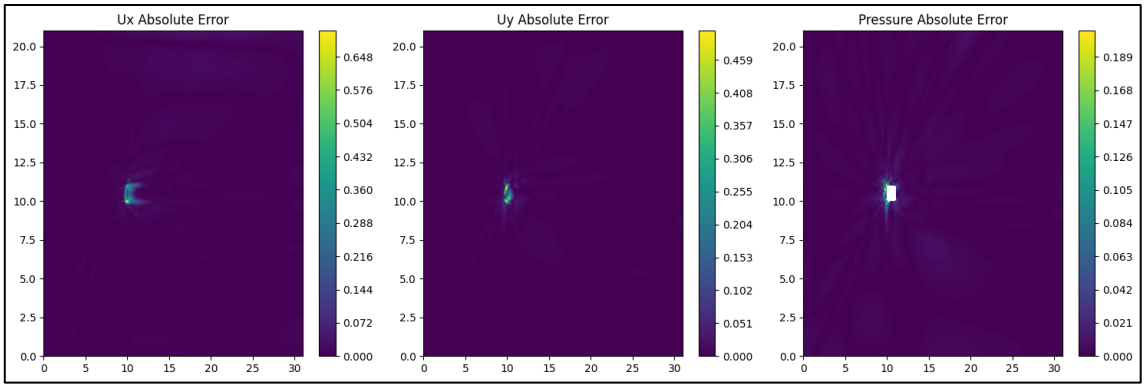

Figure 8: Absolute error contours of velocity components U_x, U_y, and pressure $p$between PINN predictions and OpenFOAM reference solutions for Re = 10.

At Re = 20 the PINN is observed to converge stably and a low final test loss of 3.1×10^{-3}. Here for u_x, MAE = 0.00398, $R^2 = 0.9979$; for v_y, MAE = 0.0018 and $R^2 = 0.991$; and for p, MAE = 0.002 with $R^2 = 0.9963$. The divergence L_2 norm reduces to 2.0×10^{-2}.

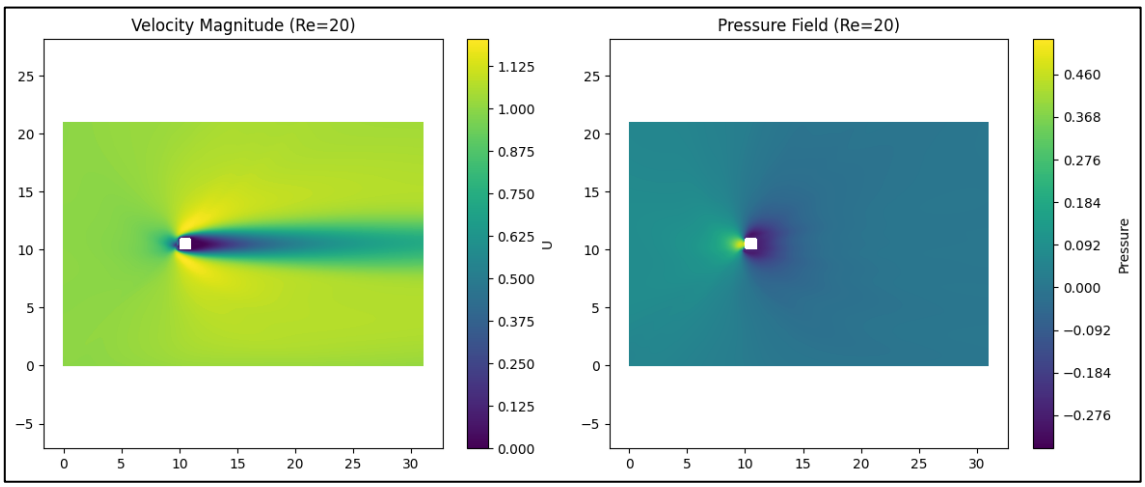

Figure 9: Velocity magnitude and pressure contours predicted by the Physics-Informed Neural Network (PINN) for Re = 20.

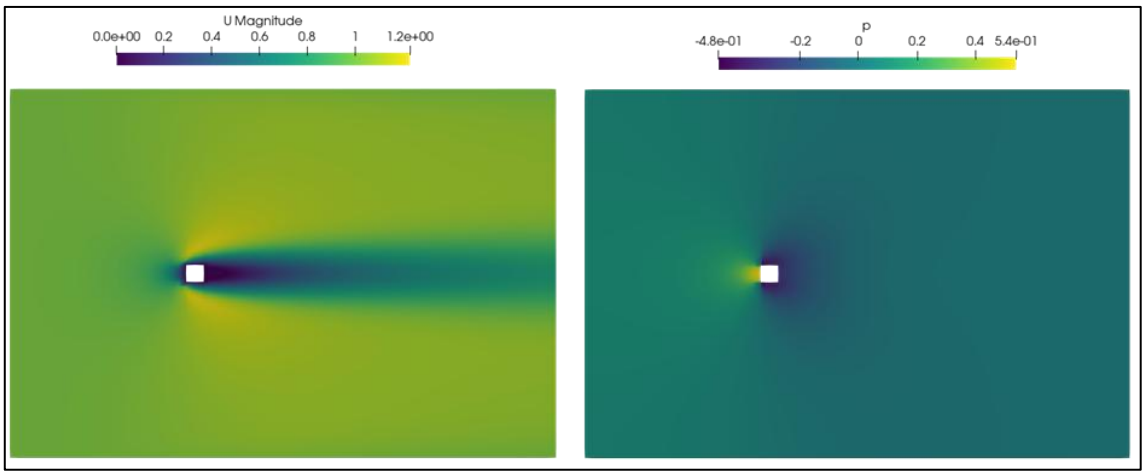

Figure 10: Velocity magnitude and pressure contours obtained from OpenFOAM simulations for Re20.

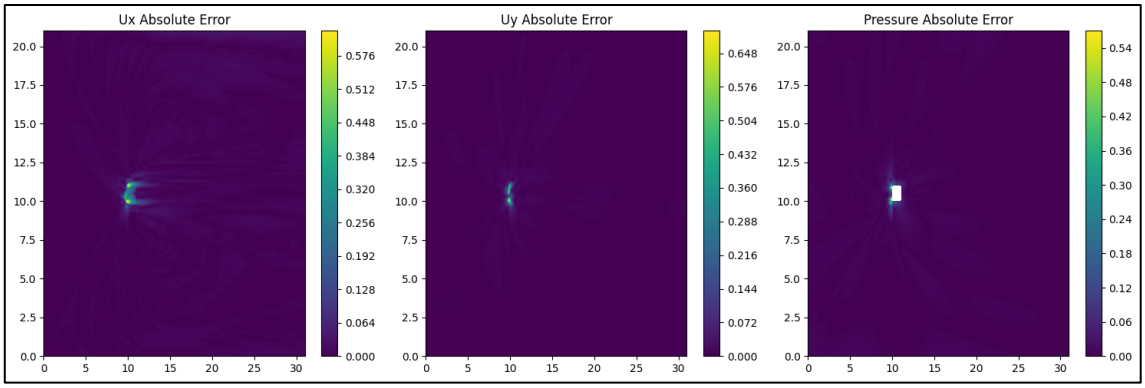

Figure 11: Absolute error contours of velocity components U_x, U_y, and pressure $p$between PINN predictions and OpenFOAM reference solutions for Re = 20.

At Re = 30, we observe a test loss of 5.3×10^{-3}. The error for u_x MAE = 0.00231, $R^2 = 0.999$; for v_y, MAE = 0.0009 and $R^2 = 0.9974$; and for p, MAE = 0.0011 with $R^2 = 0.9988$. However increase in divergence L_2 norm shows complexity in predicting flows for higher Re.

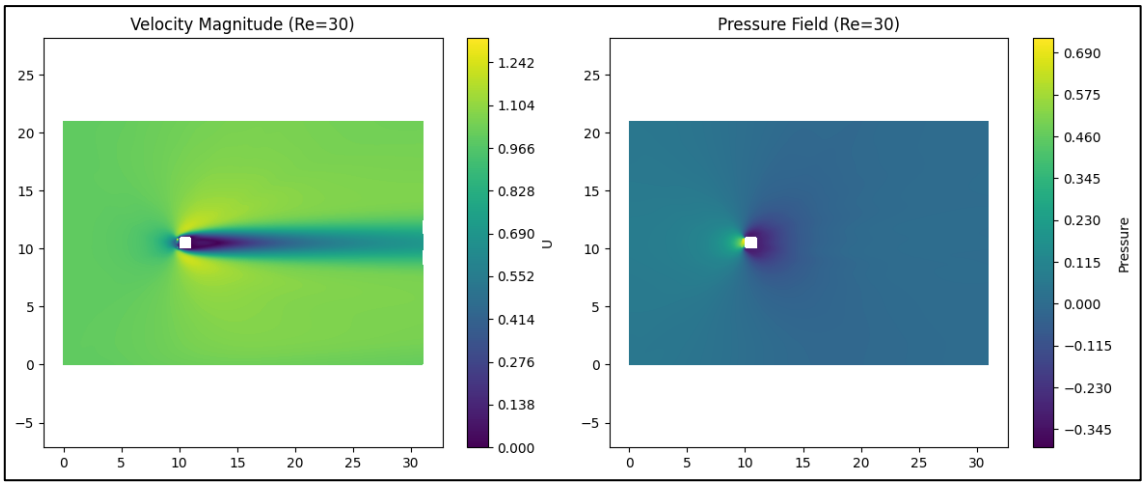

Figure 12: Velocity magnitude and pressure contours predicted by the Physics-Informed Neural Network (PINN) for Re = 30.

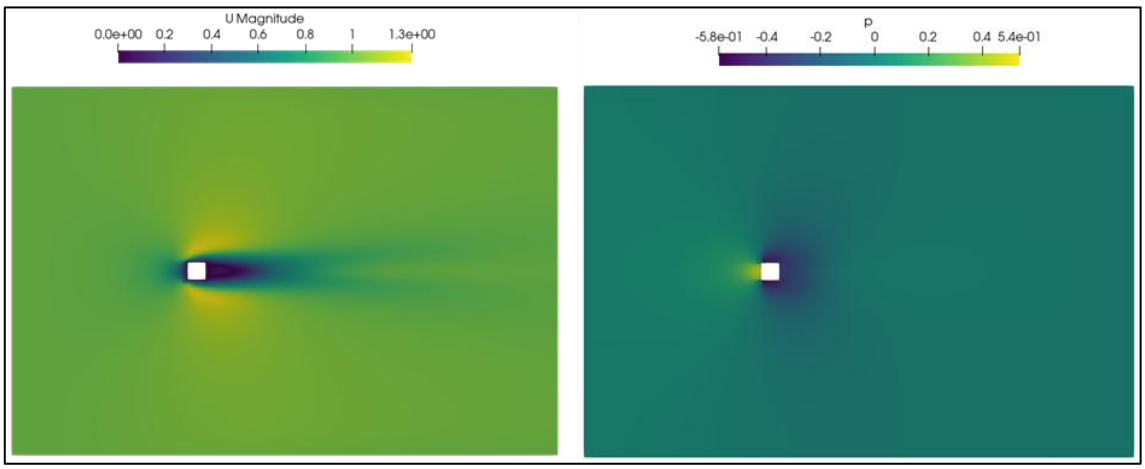

Figure 13: Velocity magnitude and pressure contours obtained from OpenFOAM simulations for Re30.

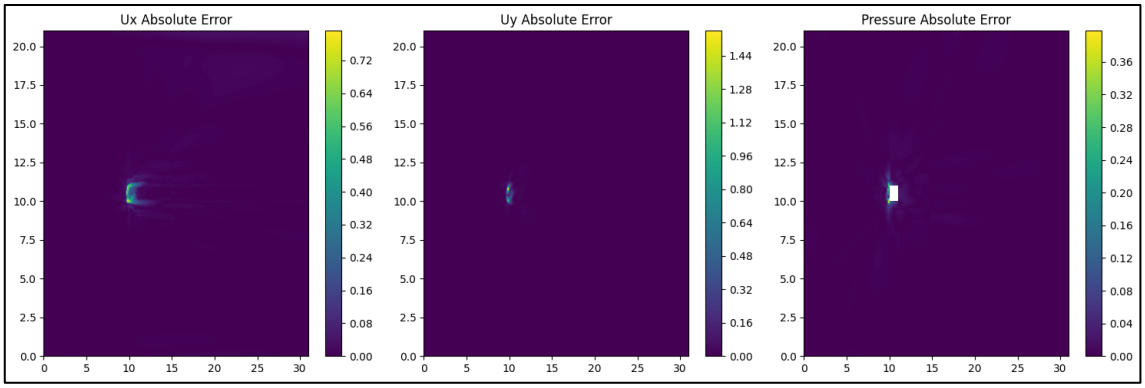

Figure 14: Absolute error contours of velocity components U_x, U_y, and pressure $p$between PINN predictions and OpenFOAM reference solutions for Re = 20.

The hybrid PINN exhibits consistent accuracy across the Reynolds number range, with all R^2 values exceeding 0.996 for primary variables. We observe that discrepancies are limited to the area around the surface of the obstacle and in the wake where gradience is high.

6. Conclusion

6.1 Summary

The present study shows that a combination of Physics-Informed Neural Networks (PINNs)-based on physical PDE residuals, boundary conditions, and high-quality CFD data- can predict accurately the steady incompressible flow around a square cylinder at Reynolds numbers 10 to 30. DeepXDE, with a 6-layer feedforward network, PINN reaches MAE < 0.004 m/s for velocity and < 0.002 Pa for pressure in test-set errors, with $R^2 > 0.996$ over all fields. The grid-less nature saves effort and time that would have been used in grid generation. The trained PINN allows for quick evaluation of flow fields at any point, thus making possible rapid analyses.

6.2 Future Work

1) Unsteady flow: Model periodic wake dynamics and Kármán vortex streets at higher Re.
2) Three-dimensional extension: Scale the hybrid PINN to 3D square cylinders or spheres to assess computational feasibility and accuracy degradation.
3) Unsteady 3D simulations: Combine temporal and spatial dimensions to capture complex spatiotemporal structures (helical vortex breakdown, instability modes) and benchmark against DNS/LES data.
4) Turbulence modelling: Integrate hybrid RANS-PINN frameworks with closure models (k-ε, k-ω) to extend applicability to high-Reynolds engineering flows.

References

[1] Raissi, M., Perdikaris, P., & Karniadakis, G. E. (2019). Physics-informed neural networks: A deep learning framework for solving forward and inverse problems involving nonlinear partial differential equations. *Journal of Computational Physics*, *378*, 686–707. https://doi.org/10.1016/j.jcp.2018.10.045

[2] Brunton, S. L., Noack, B. R., & Koumoutsakos, P. (2020). Machine learning for fluid mechanics. *Annual Review of Fluid Mechanics*, *52*, 477–508. https://doi.org/10.1146/annurev-fluid-010719-060214

[3] Cuomo, S., Di Cola, V. S., Giampaolo, F., Rozza, G., Raissi, M., & Picone, S. (2022). Scientific machine learning through physics-informed neural networks: Where we are and what's next. *Journal of Scientific Computing*, *92*, 88. https://doi.org/10.1007/s10915-022-01939-z

Appendix

Centreline Velocity Plots: We can observe that across all Reynolds numbers, the hybrid PINN predictions align closely with OpenFOAM reference solutions.

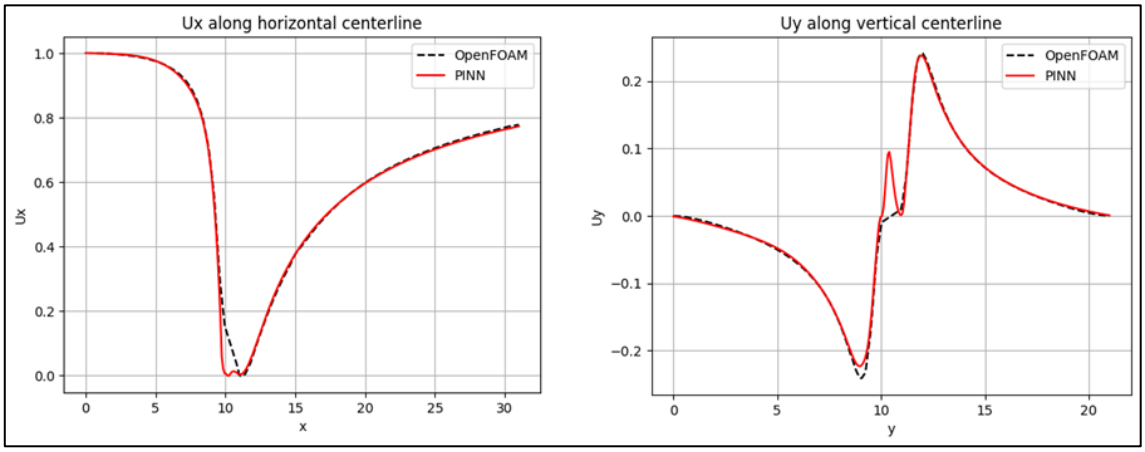

Figure A1: Centerline velocity profiles comparing PINN and OpenFOAM solutions at Re = 10.

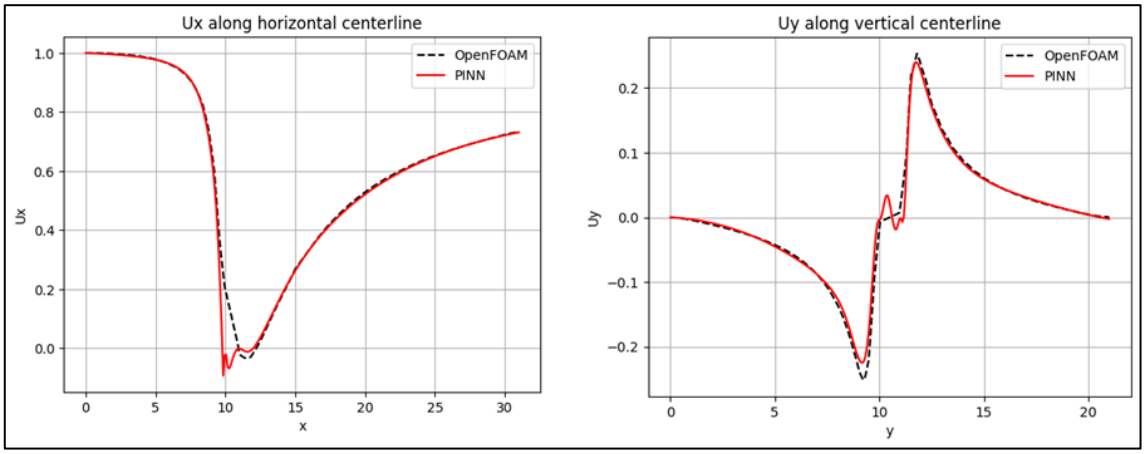

Figure A2: Centerline velocity profiles comparing PINN and OpenFOAM solutions at Re = 20.

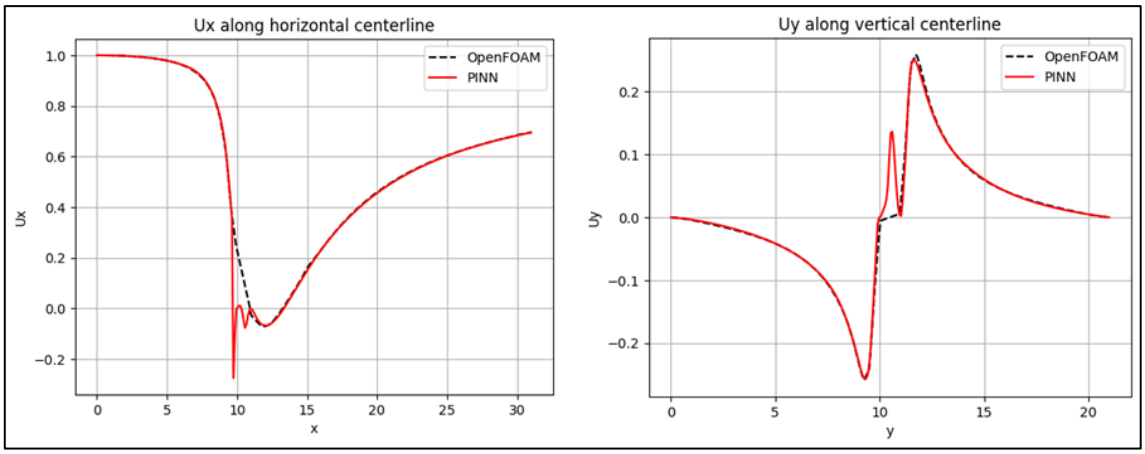

Figure A3: Centerline velocity profiles comparing PINN and OpenFOAM solutions at Re = 30.